Phase transition toward strange matter

F. Gulminelli,[1,2] Ad. R. Raduta,[3] and M. Oertel[4]
[1]*CNRS, UMR6534, LPC, F-14050 Caen Cédex, France*
[2]*ENSICAEN, UMR6534, LPC, F-14050 Caen Cédex, France*
[3]*IFIN-HH, Bucharest-Magurele, POB-MG6, Romania*
[4]*LUTH, CNRS, Observatoire de Paris, Université Paris Diderot, 5 Place Jules Janssen, 92195 Meudon, France*
(Received 21 June 2012; published 31 August 2012)

The phase diagram of a system constituted of neutrons and Λ hyperons in thermal equilibrium is evaluated in the mean-field approximation. It is shown that this simple system exhibits a complex phase diagram with first- and second-order phase transitions. Due to the generic presence of attractive and repulsive couplings, the existence of phase transitions involving strangeness appears independent of the specific interaction model. In addition we will show under which conditions a phase transition towards strange matter at high density exists, which is expected to persist even within a complete treatment including all the different strange and nonstrange baryon states. The impact of this transition on the composition of matter in the inner core of neutron stars is discussed.

DOI: 10.1103/PhysRevC.86.025805 PACS number(s): 26.50.+x, 26.60.−c, 21.65.Mn, 64.10.+h

I. INTRODUCTION

With the purpose of better understanding the dynamics of core-collapse supernova and the observed characteristics of neutron stars, a considerable theoretical effort has been undertaken in recent years concerning the modelization of the equation of state of cold dense matter [1–3] with some extensions to finite temperature; see, e.g., Refs. [4–9].

If it is well admitted that hyperonic and deconfined quark matter could exist in the inner core of neutron stars, a complete understanding of the composition and equation of state of dense matter is far from being achieved. Concerning hyperons, simple energetic considerations suggest that they should be present at high density [10]. However, in the standard picture the opening of hyperon degrees of freedom leads to a considerable softening of the equation of state [10–17], which in turns leads to maximum neutron star masses smaller than the highest values obtained in recent observations [18]. This puzzling situation implies that the hyperon-hyperon and hyperon-nucleon couplings must be much more repulsive at high density than presently assumed [19–25], and/or that something is missing in the present modelization.

Apart from neutron star observations, already for purely nuclear matter, stringent constraints on the equation of state from experimental data as well as from the theoretical side from *ab initio* calculations only exist up to roughly saturation density, mainly for almost symmetric matter at zero temperature. What makes the description of hyperonic matter even more difficult is first of all the fact that, contrary to nucleons, hyperonic data from hypernuclei (see, e.g., Refs. [26–28]), diffusion and production experiments (see, e.g., Ref. [29]) and nuclear collision experiments (see, e.g., Refs. [30,31]) are scarce. This lack of experimental information induces large uncertainties within the microscopic approaches [11–13], which suffer in addition probably from theoretical shortcomings, among others, due to the unknown hyperonic three-body forces [32]. Phenomenological extrapolations of the low-density behavior within mean-field models are subject to large uncertainties, too. In any case, there is much uncertainty on the hyperonic interactions at high density, where neutron star observations can give the only hint, though not decisive.

Here, we propose to study the phase diagram of hyperonic matter. The generic presence of attractive and repulsive couplings suggests the existence, in a model-independent manner, of a phase transition involving strangeness. In order to have an analytically solvable model, we consider the simplified situation where only neutrons, n, and Λ hyperons are allowed in the matter chemical composition. We find, as argued above, a first-order phase transition involving strangeness. In addition, we will show under which assumptions on the ΛΛ and $n\Lambda$ interactions, respecting the available constraints, a phase transition towards strange matter, that is, with a discontinuity in the strangeness content of matter, exists at high density.

We leave the inclusion of protons and higher mass strange and nonstrange baryons to a future study. Because of this simplification, we will not be able to exploit the results for a predictive quantitative application to neutron stars and dense supernova matter. However, this simplification will allow us to have an exactly solvable model with perfectly controlled numerics. We believe that the relevant degrees of freedom to explore the opening of the strangeness channels are included already at this level, and the qualitative features of the strangeness phase transition will not change in the complete model.

Concerning the phenomenological consequences of our findings, let us stress that many published works on hyperonic matter make use of the mean-field approximation (e.g., Refs. [10,14,17,19–25]). However, if the opening of the strangeness degree of freedom at high baryonic density is associated with a first-order phase transition, the mean-field equations of state should be modified making use of the Gibbs construction [33]. The possible presence of coexisting phases would in addition modify the matter composition with respect to the uncorrected mean-field predictions [34–36].

Both matter composition and equation of state are important ingredients, not only in the calculations of neutrons star

TABLE I. Different parameter sets for the nn, $n\Lambda$, and $\Lambda\Lambda$, interactions from Ref. [39] (BGI, BGII, and BGIII) and Ref. [25] (220g2.8).

Parameter set	a_{NN} (MeV fm^3)	b_{NN} (MeV fm^3)	c_{NN} (MeV fm$^{3\delta}$)	$a_{\Lambda\Lambda}$ (MeV fm^3)	$c_{\Lambda\Lambda}$ (MeV fm$^{3\gamma}$)	$a_{\Lambda N}$ (MeV fm^3)	$c_{\Lambda N}$ (MeV fm$^{3\gamma}$)	δ	γ
BGI	−784.4	214.2	1936.0	−486.2	1553.6	−340.0	1087.5	2	2
BGII	−935.4	214.2	1557.2	−552.6	1055.4	−387.0	738.8	5/3	5/3
BGIII	−1384.6	214.2	1672.8	−723.2	869.0	−505.2	605.5	4/3	4/3
220g2.8	−1636.2	214.2	1869.26	−400	1500	−270	2300	1.26	2.8

models, but in the hydrodynamical codes describing core collapse dynamics, too. The high-density and high-temperature behavior not only influences the success of the explosion, but among other factors also influences the dependence of the final state (neutron star or black hole) on the progenitor mass (see, e.g., Refs. [37,38]). This means that the possible presence of a phase transition toward strange matter has to be studied at finite temperature, too.

II. THE MODEL

In the following we will illustrate the propositions concerning the phase diagram by choosing a specific interaction model for the $n\Lambda$ system. Of course, the quantitative numerical results are not model independent, but we will argue why our findings on the phase diagram are general.

The energetics of the $n\Lambda$ mixture is described through the energy density functional proposed by Balberg and Gal [39],

$$\begin{aligned}\epsilon_{\rm pot}(\rho_n,\rho_\Lambda) = {} & \tfrac{1}{2}\left[(a_{NN}+b_{NN})\rho_n^2 + c_{NN}\rho_n^{\delta+1}\right] \\ & + \tfrac{1}{2}\left[a_{\Lambda\Lambda}\rho_\Lambda^2 + c_{\Lambda\Lambda}\rho_\Lambda^{\gamma+1}\right] + a_{\Lambda n}\rho_n\rho_\Lambda \\ & + c_{\Lambda n}\tfrac{\rho_n\rho_\Lambda}{\rho_n+\rho_\Lambda}\left[\rho_n^\gamma + \rho_\Lambda^\gamma\right], \end{aligned} \tag{1}$$

where the interaction couplings, compatible with the Lattimer-Swesty equation of state in the nonstrange sector, are given in Table I. Parametrizations BGI, BGII and BGIII are taken from the work by Balberg and Gal [39] and 220g2.8 corresponds to one of the parametrizations compatible with the observation of an almost two-solar-mass neutron star [18] from Ref. [25]. In the applications shown below we will use mainly parametrization BGI, but we have performed the calculations for the other parameter sets, too.

In the nonrelativistic mean-field approximation the kinetic energy density $\epsilon_{\rm kin} = \epsilon_{{\rm kin},n} + \epsilon_{{\rm kin},\Lambda}$ has the simple ideal Fermi gas form

$$\epsilon_{{\rm kin},q} = \frac{2\pi}{\beta h^3}(2s_q+1)\left(\frac{2m_q^*}{\beta}\right)^{3/2}\int_0^\infty dx\,\frac{x^{3/2}}{1+\exp(x-\beta\tilde{\mu}_q)}, \tag{2}$$

where $q = n, \Lambda$, s_q is the particle spin, $\beta = T^{-1}$ is the inverse temperature, $m_q^* = m_q$ for the chosen interaction parameters, and the Fermi integral depends on an effective chemical potential $\tilde{\mu}_q = \mu_q - U_q - m_q c^2$, shifted with respect to the thermodynamic chemical potential because of the rest mass and the depth of the self-consistent mean field $U_q \equiv \partial\epsilon_{\rm pot}/\partial\rho_q$. At zero temperature the Fermi integral can be analytically solved, giving

$$\epsilon_{{\rm kin},q}(T=0) = \frac{\hbar^2}{2m_q^*}\frac{3}{5}\rho_q\left(\frac{6\pi^2\rho_q}{2s_q+1}\right)^{2/3}. \tag{3}$$

The energy density $\epsilon = \epsilon_{\rm kin} + \epsilon_{\rm pot}$ at zero temperature obtained with the parameter set BGI for different hyperon fractions $Y_\Lambda = \rho_\Lambda/(\rho_\Lambda+\rho_n)$ is represented in Fig. 1. We can see that pure neutron matter, as well as pure Λ matter, are never bound. For pure neutron matter this is well known. For pure Λ matter it is less obvious, since it involves the $\Lambda\Lambda$ interaction, subject to large uncertainties. A strong attraction at low densities could alter this result. We think, however, that this is not the case, since parameter set I by Balberg and Gal [39], shown in Fig. 1, assumes a much stronger attraction than indicated by more recent analysis [40]. There is almost no doubt that the $n\Lambda$ interaction should be attractive at low densities and repulsive at high densities. Due to the attractive part of the $n\Lambda$ coupling, a mixture of the two particle species admits a bound state at finite density. This rather general feature of the energy density is found within the other parametrizations and other models, e.g., the parametrization of the energy density functional from G-matrix calculations by Vidana *et al.* [41]. Within parametrization BGI, the lowest energy corresponds to a symmetric mixture $\rho_n = \rho_\Lambda$ and a bound state is predicted for $0.19 < Y_\Lambda < 0.85$.

The existence of a minimum in the energy functional for symmetric matter means that such a state represents the stable matter phase at zero temperature. On the other side, the

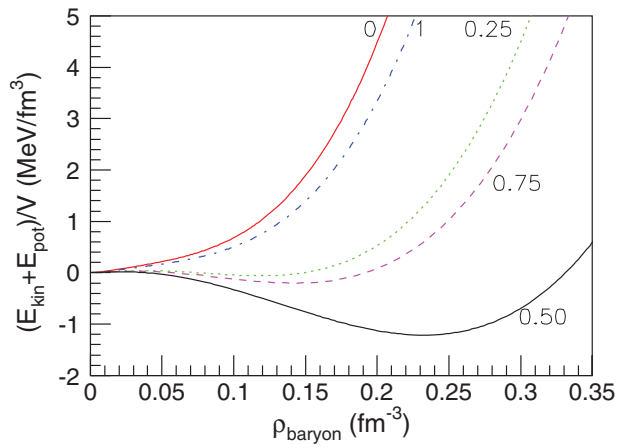

FIG. 1. (Color online) Energy density as a function of the total baryon density for a (n, Λ) mixture at $T = 0$ with different Λ fractions as obtained by the parameter set BGI.

vanishing density gas phase is always the stable phase in the limit of infinite temperature. This implies that a dilute-to-dense phase change implying strangeness has to be expected on very general grounds. The presence of a minimum is however not sufficient to discriminate between a smooth crossover and a phase transition. In the next section we will therefore demonstrate the existence of a phase transition by explicitly calculating the $n\Lambda$ phase diagram.

III. PHASE DIAGRAM OF THE TWO-COMPONENT $n\Lambda$ SYSTEM

First-order transitions are signaled by an instability or concavity anomaly in the mean-field thermodynamic potential, which has to be cured by means of the Gibbs phase equilibrium construction at the thermodynamic limit. For this reason the convexity analysis of the thermodynamical potential in the extensive variable space has been often employed to spot the presence of phase transitions, e.g., for the neutron-proton system [42,43]. At zero temperature, one thermodynamic potential is given by the total energy

$$\epsilon_{\rm tot}(\rho_n,\rho_\Lambda)=\epsilon_{\rm pot}(\rho_n,\rho_\Lambda)+\epsilon_{\rm kin}(\rho_n,\rho_\Lambda)+(\rho_n m_n+\rho_\Lambda m_\Lambda)c^2, \quad (4)$$

and the curvature matrix is defined by

$$\begin{pmatrix} C_{nn} & C_{n\Lambda} \\ C_{\Lambda n} & C_{\Lambda\Lambda}\end{pmatrix}=\begin{pmatrix} \frac{\partial^2 e_{\rm tot}}{\partial\rho_n^2} & \frac{\partial^2 e_{\rm tot}}{\partial\rho_n\partial\rho_\Lambda} \\ \frac{\partial^2 e_{\rm tot}}{\partial\rho_\Lambda\partial\rho_n} & \frac{\partial^2 e_{\rm tot}}{\partial\rho_\Lambda^2}\end{pmatrix}=\begin{pmatrix} \frac{\partial\mu_n}{\partial\rho_n} & \frac{\partial\mu_n}{\partial\rho_\Lambda} \\ \frac{\partial\mu_\Lambda}{\partial\rho_n} & \frac{\partial\mu_\Lambda}{\partial\rho_\Lambda}\end{pmatrix}, \quad (5)$$

with $C_{n\Lambda}=C_{\Lambda n}$ and real eigenvalues $C_{\rm min}<C_{max}$. The spinodal region is then recognized as the locus of negative curvature of the energy surface, $C_{\rm min}<0$. The corresponding eigenvector defines a direction in the density space given by

$$\frac{\rho_n}{\rho_\Lambda}=\frac{C_{n\Lambda}}{C_{\rm min}-C_{nn}}=\frac{C_{\rm min}-C_{\Lambda\Lambda}}{C_{\Lambda n}}. \quad (6)$$

This instability direction physically represents the chemical composition of density fluctuations which are spontaneously and exponentially amplified in the unstable region in order to achieve phase separation, and gives the order parameter of the associated phase transition. In all the parametrizations we have analyzed, one of the eigenvalues is always positive, meaning that the order parameter of the $n\Lambda$ transition is always one-dimensional, similar to the liquid-gas nuclear phase transition at subsaturation densities.

The zero-temperature instability region of the $n\Lambda$ mixture is shown in Fig. 2 with parameter set BGI. We can see that a large portion of the phase diagram is concerned by the instability. We can qualitatively distinguish three regions characterized by different order parameters. Below nuclear saturation density, we observe an isoscalar $\rho_n\approx\rho_\Lambda$ instability, very close to ordinary nuclear liquid-gas, with Λ's playing the role of protons. This could have been expected, due to the similarity between the energy density for $Y_\Lambda=0.5$ (cf. Fig. 1) and the well known energy density for low-density np matter. Neutron matter close to saturation is stabilized by the inclusion of a nonzero Λ fraction, which is consistent with the observation that the neutron drip line is shifted toward more neutron-rich systems in hypernuclei [44].

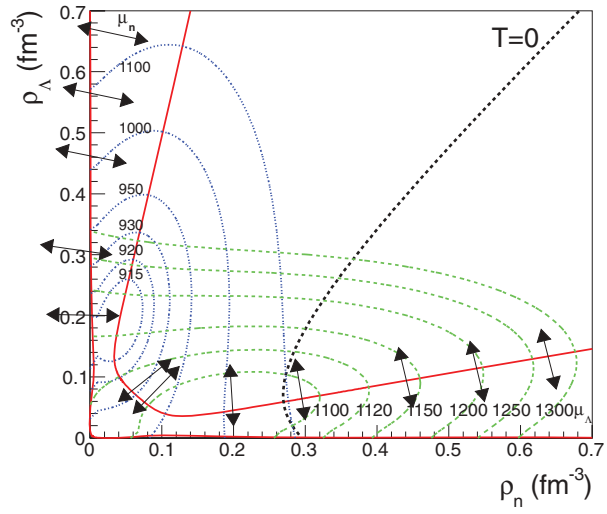

FIG. 2. (Color online) Frontiers of the spinodal instability domain of the (n,Λ) mixture at $T=0$ (thick red solid lines) corresponding to the parameter set BGI; trajectories of constant μ_n (blue dotted lines) and constant μ_Λ (green dashed lines); the arrows indicate the directions of phase separation; the (black) short-dashed line illustrates the $\mu_S=0$ trajectory associated to the equilibrium of strangeness.

With increasing neutron density the phase separation progressively changes toward the strangeness $\rho_S=-\rho_\Lambda$ direction: the two stable phases connected by the instability have close baryon densities but a very different fraction of Λ's. For high ρ_Λ we observe the same behavior with the roles of neutrons and Λ hyperons exchanged. The part of the phase diagram at high neutron density comprises the region physically explored by supernova and neutron star matter, which is characterized by chemical equilibrium for reactions implying strangeness, $\mu_S=\mu_n-\mu_\Lambda=0$. The strangeness equilibrium trajectory is represented by a dashed line in Fig. 2. This physically corresponds to the sudden opening of strangeness, observed in many modelizations of neutron star matter (see, e.g., Ref. [17,39]).

Assuming the order parameter to be given exactly by ρ_S, which is a very good approximation at high ρ_n, we can understand the existence of this high-density strangeness phase transition in terms of the $n\Lambda$ and $\Lambda\Lambda$ interactions. Under this assumption, the curvature analysis can be performed one-dimensionally, as a function of ρ_Λ only. Thus the instability region is determined mainly by the condition $C_{\Lambda\Lambda}<0$. In Fig. 3 the Λ chemical potential, with the constant mass subtracted, that is, the first derivative of the energy density with respect to ρ_Λ, is displayed for parametrization BGI. A minimum in μ_Λ is related to a zero in the curvature in the strangeness direction, indicating thus the border of an instability region. This minimum is clearly visible in Fig. 3. It is more pronounced with increasing neutron density and shifted to higher values of ρ_Λ. Apart from the trivial kinetic term $\sim\rho_\Lambda^{2/3}$, μ_Λ contains the Λ single-particle potential, $U_\Lambda(\rho_\Lambda,\rho_n)=\partial\epsilon_{\rm pot}/\partial\rho_\Lambda$, thus reflecting the $n\Lambda$ and $\Lambda\Lambda$ interactions. Within the model by Balberg and Gal [39], the

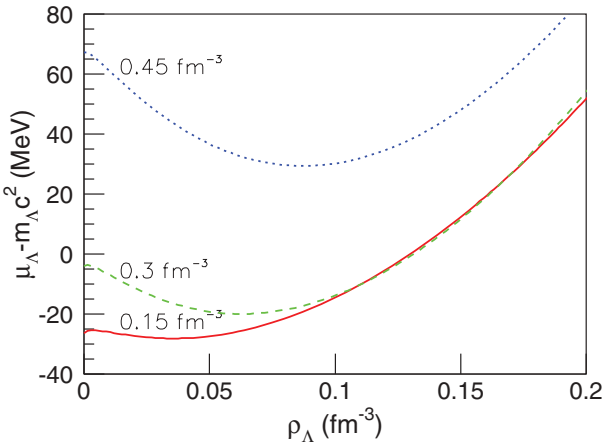

FIG. 3. (Color online) Strangeness chemical potential as a function of strangeness density, $\rho_s = -\rho_\Lambda$, for different neutron densities at $T = 0$. The considered parameter set is BGI.

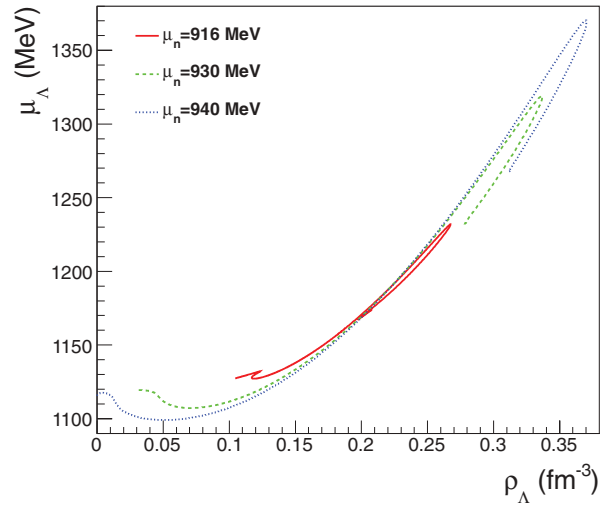

FIG. 4. (Color online) Λ chemical potential as a function of the associated density ρ_Λ at $T = 0$ for different values of $\mu_n = 916$, 930, and 940 MeV and parameter set BGI.

attractive part of the $\Lambda\Lambda$ interaction and the specific form of the $n\Lambda$ interaction contribute to this minimum.

Let us stress that the central region of the instability domain, below roughly saturation density, is determined mainly by the fact that pure neutron (and Λ) matter is unbound and there is low-density attraction in the $n\Lambda$ channel. The finding in this region thus seems qualitatively robust. The existence of a strangeness phase transition at high density, on the contrary, is not a general model-independent feature, although, as mentioned above, many models show it. There are others, for instance the G-matrix models of Refs. [16,41], which do not show an instability in this region. This can be seen from the absence of a minimum in μ_Λ as a function of ρ_Λ for constant ρ_n. The reason is twofold: first, a $\Lambda\Lambda$ interaction is completely missing from these models and, second, the $n\Lambda$ interaction has a slightly different form than that of Balberg and Gal [39]. Owing to the lack of reliable information on the hyperonic interactions, which would discriminate between different models, we cannot affirm the existence of the strangeness phase transition related to this instability, but, turning the argument around, the presence of this phase transition in a physical system would allow us to learn much about the shape of the interaction.

One remark of caution concerning the relation of the instability domain with a phase transition is in order here. In principle, the presence of an instability is a pathology of mean-field approaches. It is an indication that the lowest energy (or free energy at finite temperature) equilibrium solution is different from the unstable mean-field one. If the equilibrium solution corresponds to macroscopic dishomogeneities, it can and it should be recovered from the mean-field results, making use of the Gibbs construction. In this case the convexity in the curvature matrix reflects a physical instability toward phase separation, and the phase diagram contains a region of phase coexistence. However, since the mean-field equations of state are by construction analytic infinitely differentiable functions, it is possible that the instability is due to a multiple evaluation of densities in a given point of the phase diagram defined by the set of associated chemical potentials, too. This may not be pertinent in our simple model allowing only two different particle species, but might very well occur in a more complete model including all hyperons and resonance states [39]. In this case the unstable solution has to be eliminated from the equilibrium landscape, without necessarily any phase transition occurring.

To discriminate between the two scenarios and correct the mean-field instabilities, one has therefore to study the phase diagram in the space of chemical potentials. A useful trick to spot phase transitions with more than one conserved charge is to perform a Legendre transform to the statistical ensemble where all extensive variables but one are replaced by their conjugated intensive Lagrange parameters [45]. In this ensemble the multidimensional Gibbs equilibrium conditions reduce to a simple Maxwell construction.

In our simple two-dimensional case we can work equivalently within the ensemble where the neutron density is controlled, or, alternatively, within the ensemble where the Λ density is controlled, corresponding to the two constrained energies

$$\begin{aligned} \bar{e}_{\mu_\Lambda}(\rho_n) &= e_{\rm tot}(\rho_\Lambda, \rho_n) - \mu_\Lambda \rho_\Lambda, \\ \bar{e}_{\mu_n}(\rho_\Lambda) &= e_{\rm tot}(\rho_\Lambda, \rho_n) - \mu_n \rho_n. \end{aligned} \tag{7}$$

Let us concentrate on the second representation. The behavior of the Λ chemical potential, $\mu_\Lambda \equiv \partial \bar{e}_{\mu_n}/\partial \rho_\Lambda$, is shown for some selected values of the neutron chemical potential in Fig. 4. At variance with the well known nonstrange nuclear matter np system, equilibrium can only be defined within a finite interval of density. Indeed the ending points of the curves correspond to vanishing neutron density, as can be seen from the iso-μ contours in Fig. 2.

At relatively high neutron chemical potential the curves present a back-bending at low Λ densities, similar to the usual Van der Waals phenomenology for the fluid transition at finite temperature. In this case the mean-field solution is unique, but a more stable solution is obtained by phase mixing. At low μ_n values and, independent of μ_n, in the high-density

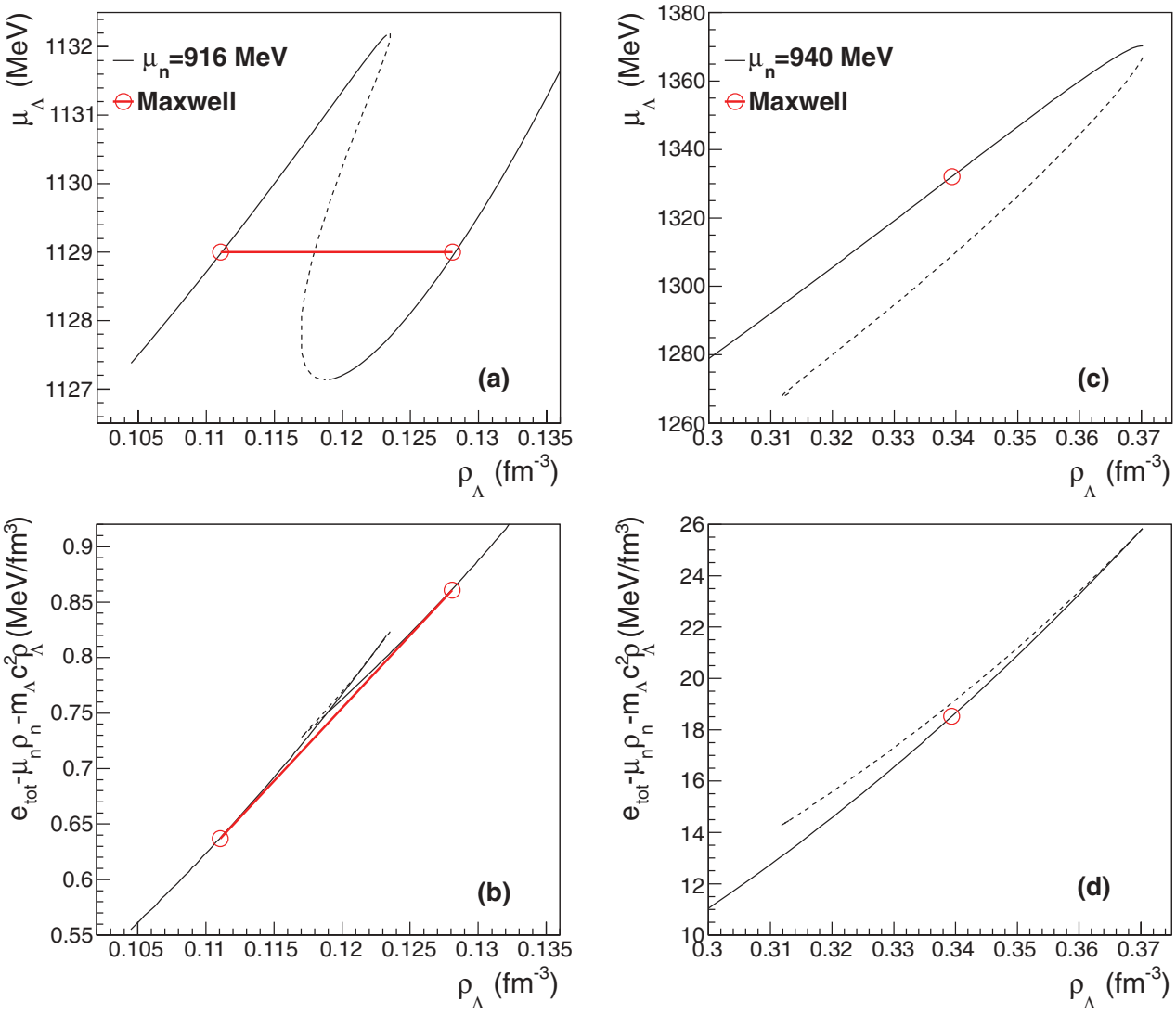

FIG. 5. (Color online) Upper part: zoom-in on the low (left) and high (right) density domains of $\mu_\Lambda(\rho_\Lambda)|_{\mu_n}$ for $\mu_n = 916$ MeV (left) and $\mu_n = 940$ MeV (right). Lower part: associated constrained energy. In case of multiple evaluation, the unfavored solution(s) are represented with a dashed line. The red open circles and line mark the convex envelope defined by the Gibbs construction. For the density energy functional we have used BGI.

region, multiple evaluations are observed, where different values of μ_Λ are compatible with the same controlled value of the hyperon density. In this situation, only the solution leading to the lowest constrained energy has to be retained. To explore these different possibilities, a zoom-in of Fig. 4 for $\mu_n = 916$ MeV is shown in Fig. 5, together with the associated thermodynamic potential. For better visibility, the rest-mass contribution $m_\Lambda c^2 \rho_\Lambda$ has been subtracted, which does not alter the convexity properties of the function. We can see that, at low density, after elimination of the least stable solution, the constrained energy can still be minimized by taking a linear combination of two homogeneous solutions (circles in Fig. 5) having the same first-order derivative, that is, the same chemical potential. Since these two points have the same value for all the intensive variables (μ_n, μ_Λ, T), they respect Gibbs equilibrium rules. One can therefore see that the ensemble of Maxwell constructions in the (μ_n, ρ_Λ) ensemble is equivalent to the construction of the global convex envelope of the energy, that is, to the Gibbs construction of the complete system.

In the high density case (right part of Fig. 5), the elimination of the multiple evaluation leaves a monotonous equation of state, which does not allow any energy gain by linear interpolations. Going back again to the iso-μ curves of Fig. 2, we can see that the high-ρ_Λ region corresponding to the bi-evaluation can also be explored in the complementary (μ_Λ, ρ_n) ensemble where it will be associated with low values of ρ_n. This means that, from a practical point of view, once the phase mixing is systematically performed on the low-density (ρ_Λ and ρ_n) region, all the unstable mean-field solutions turn out to be automatically removed.

The final result of the Gibbs construction is given in Fig. 6 together with the corrected iso-μ_n paths. We can see

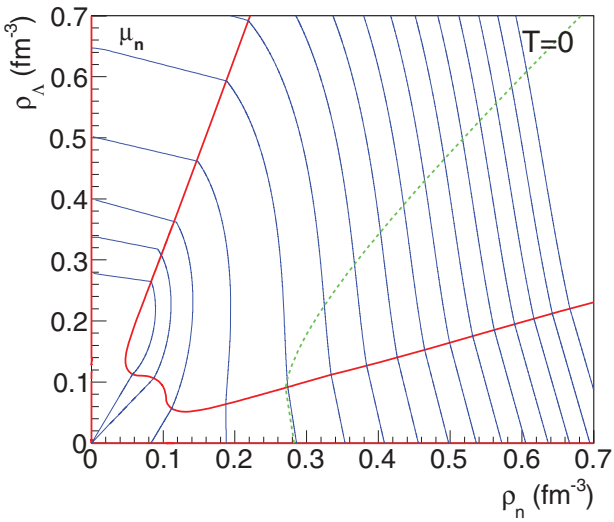

FIG. 6. (Color online) (n, Λ) mixture at $T = 0$: borders of the phase coexistence region (red thick lines), constant-μ_n paths after Maxwell construction (blue thin lines), and $\mu_n = \mu_\Lambda$ trajectory after Maxwell construction (dark green dashed line). From left to right, the considered values of μ_n are 920, 930, 950, 1000, 1100, 1200, 1300, 1400, 1500, 1600, 1700, 1800, 1900, 2000, 2100, and 2200 MeV. The considered parameter set is BGI.

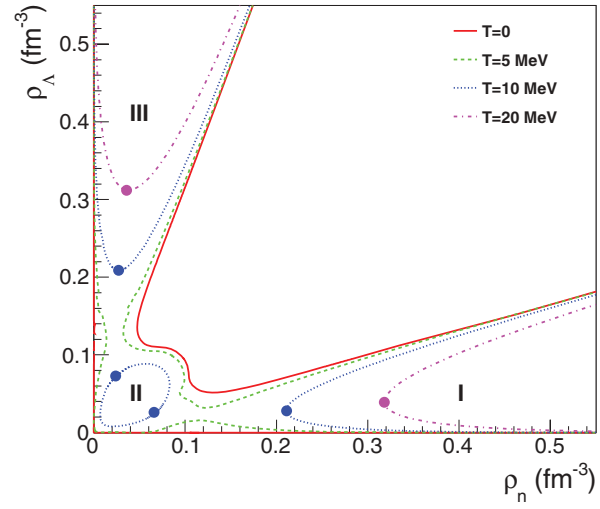

FIG. 7. (Color online) Borders of the phase coexistence region of the $n\Lambda$ mixture for different temperatures, $T = 0, 5, 10$, and 20 MeV, and parameter set BGI. The full circles mark the critical points.

that the whole unstable region of Fig. 2 can be interpreted as the spinodal region of a first-order phase transition. In particular, if we follow the physical path $\mu_n = \mu_\Lambda$ associated with equilibrium of strangeness (dashed line in Fig. 6), the emergence of strangeness with the opening of the hyperon channel corresponds to the mixed-phase region of a first-order phase transition, which is not correctly modeled in the mean-field approximation.

Up to now we have only presented results at zero temperature. The extension to finite temperature, which is needed for supernova matter, is relatively simple in the mean-field approximation. The appropriate thermodynamic potential at nonzero temperature is given by the Helmholtz free energy

$$f_T(\rho_n, \rho_\Lambda) = \epsilon_{\rm tot}(\rho_n, \rho_\Lambda) - T s(\rho_n, \rho_\Lambda), \tag{8}$$

where s is the mean-field entropy density. Chemical potentials can be obtained by differentiating this expression or, in a simpler numerical way, by inverting the Fermi integral associated with the densities [46] from the two coupled equations:

$$\rho_q = \frac{2\pi}{h^3}(2s_q + 1)\left(\frac{2m_q^*}{\beta}\right)^{3/2}\int_0^\infty dx \frac{x^{1/2}}{1 + \exp(x - \beta\tilde{\mu}_q)}, \tag{9}$$

with $q = n, \Lambda$. Then the Gibbs construction is performed, as in the zero-temperature case, from the combined analysis of $\mu_n(\rho_n)$ at constant μ_Λ, and $\mu_\Lambda(\rho_\Lambda)$ at constant μ_n. The same qualitative behaviors as in Fig. 4 are observed, with the difference that at finite temperature chemical potentials tend to $-\infty$ with vanishing density. As a consequence, the lower energy border of the coexistence zone is always at finite nonzero density, and Gibbs constructions are always equivalent to equal-area constructions in the mono-extensive ensemble.

The phase diagram as a function of the temperature is presented in Fig. 7. This phase diagram exhibits different interesting features. We can see that the three regions that we have tentatively defined at zero temperature appear as distinct phase transitions at finite temperature. The first phase transition (zone II in Fig. 7) separates a low-density gas phase from a high-density more symmetric liquid phase, very similar to ordinary liquid-gas. The second one (zone III in Fig. 7) reflects the instability of dense strange matter toward the appearance of neutrons and has an almost symmetric counterpart (zone I in Fig. 7) in the instability of dense neutron matter toward the formation of Λ hyperons. Up to a certain temperature, this latter phase transition is explored by the $\mu_n = \mu_\Lambda$ trajectory, meaning that it is expected to occur in neutron stars and supernova matter. At variance with other known phase transitions in nuclear matter, this transition exists at any temperature and is not limited in density; it is always associated (except at $T \lesssim 5$ MeV in the present model) with a critical point, which moves toward high density as the temperature increases. This means that criticality should be observed in hot supernova matter, at a temperature which is estimated as $T_c = 14.8$ MeV in the present schematic model.

The consequences of these findings for the composition of neutron star matter are drawn in Fig. 8. The left panel shows the Λ fraction $Y_\Lambda = \rho_\Lambda/(\rho_n + \rho_\Lambda)$ as a function of the baryon density under the condition $\mu_n = \mu_\Lambda$ at $T = 0$. The crossing of the mixed-phase region with increasing neutron density implies that, as soon as the lower density transition border is crossed, the system has to be viewed as a dishomogeneous mixture of macroscopic regions composed essentially of neutrons, with other macroscopic regions with around 25% hyperons. The extension of the Λ-rich zone increases with density until the system exits the coexistence zone, and becomes homogeneous again.

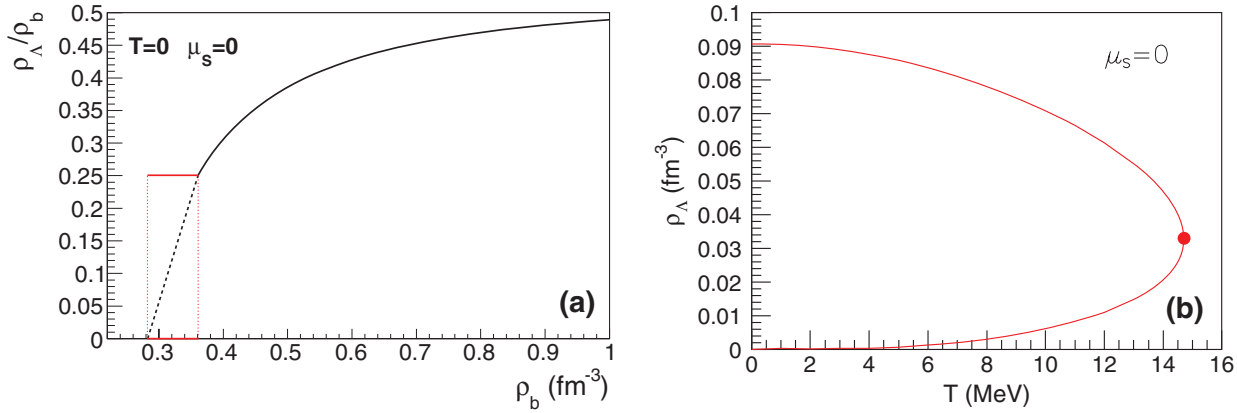

FIG. 8. (Color online) Left: Λ fraction as a function of the baryon density within the condition $\mu_n = \mu_\Lambda$ for a $n\Lambda$ mixture at $T = 0$. The full line corresponds to the stable mean-field results; the dashed line illustrates the Gibbs construction; the horizontal lines indicate the relative amount of Λ hyperons at the frontiers of the phase-coexistence domain. Right: Λ density for the two coexisting phases as a function of temperature for $\mu_S = 0$. As before, we have used BGI.

On the right panel of Fig. 8 the Λ densities for the two coexisting phases are displayed as a function of temperature, again under the condition of $\mu_n = \mu_\Lambda$, physically relevant for neutron star and supernova matter. The extension of the coexistence region decreases with increasing temperature. The latter finally disappears at $T_c = 14.8$ MeV. This well illustrates the fact already observed in connection with the phase diagram, cf. Fig. 7, that the critical point of the strangeness phase transition moves to higher density, crossing the physical line $\mu_n = \mu_\Lambda$ at a given temperature, $T_c = 14.8$ MeV in the present example.

IV. CONCLUSIONS

In this paper we have calculated the phase diagram of an interacting system of neutrons and Λ hyperons in the mean-field approximation. We have shown that this simple system presents a complex phase diagram with first- and second-order phase transitions. Some of these phase transitions are probably never explored in physical systems. However, a possible phase transition at supersaturation baryon densities, from nonstrange to strange matter, is expected to be observed both in the inner core of neutron stars and in the dense regions of core-collapse supernovas. For this latter phenomenology, a critical point is predicted and the associated critical opalescence could have an impact on supernova dynamics [47]. The existence of this particular phase transition can be related to the form of the ΛΛ and $n\Lambda$ interactions and is, in the present model, essentially due to the presence of an attractive low-density ΛΛ interaction as well as to the high-density part of the $n\Lambda$ interaction. As such, it is expected to persist in a realistic model of dense matter including more hyperonic and nonhyperonic baryons. The immediate consequence of that is that the opening of hyperon channels at high density should not be viewed as a continuous (though abrupt) increase of strangeness in the matter, observed in many models of hyperonic matter—cf., e.g., Ref. [17]—but rather as the coexistence of hyperon-poor and hyperon-rich macroscopic domains.

Different steps have, however, to be achieved before quantitative predictions on neutron star physics can be drawn from this simple model. The model should be extended to include all possible hyperons and resonances, which could shift the coexistence borders and induce new phenomena in the direction—not explored in this preliminary study—of the electric charge density. These improvements will be the object of a future publication.

ACKNOWLEDGMENTS

This paper has been partly supported by the ANR under the project NEXEN and the project SN2NS, ANR-10-BLAN-0503, and by IFIN-IN2P3 agreement No. 07-44. Support from Compstar, a research networking program of the European Science foundation, is acknowledged, too. Ad.R.R. acknowledges partial support from the Romanian National Authority for Scientific Research under Grant No. PN-II-ID-PCE-2011-3-0092 and kind hospitality from LPC-Caen.

[1] M. Prakash, I. Bombaci, M. Prakash, P. J. Ellis, J. M. Lattimer, and R. Knorren, Phys. Rep. **280**, 1 (1997).
[2] J. M. Lattimer and M. Prakash, Phys. Rep. **442**, 109 (2007).
[3] A. Sedrakian, Prog. Part. Nucl. Phys. **58**, 168 (2007).
[4] J. M. Lattimer and F. D. Swesty, Nucl. Phys. A **535**, 331 (1991).
[5] H. Shen, H. Toki, K. Oyamatsu, and K. Sumiyoshi, Nucl. Phys. A **637**, 435 (1998).
[6] M. Hempel and J. Schaffner-Bielich, Nucl. Phys. A **837**, 210 (2010).
[7] S. I. Blinnikov, I. V. Panov, M. A. Rudzsky, and K. Sumiyoshi, Astron. Astrophys. **535**, A37 (2011).
[8] S. Heckel, P. P. Schneider, and A. Sedrakian, Phys. Rev. C **80**, 015805 (2009).
[9] Ad. R. Raduta and F. Gulminelli, Phys. Rev. C **82**, 065801 (2010).

[10] N. Glendenning, Phys. Lett. B **114**, 392 (1982).
[11] M. Baldo, G. F. Burgio, and H. J. Schulze, Phys. Rev. C **61**, 055801 (2000).
[12] I. Vidana, A. Polls, A. Ramos, L. Engvik, and M. Hjorth-Jensen, Phys. Rev. C **62**, 035801 (2000).
[13] H. Djapo, B. J. Schaefer, and J. Wambach, Phys. Rev. C **81**, 035803 (2010).
[14] J. R. Stone, P. A. M. Guichon, and A. W. Thomas, arXiv:1012.2919.
[15] H.-J. Schulze and T. Rijken, Phys. Rev. C **84**, 035801 (2011).
[16] G. F. Burgio, H.-J. Schulze, and A. Li, Phys. Rev. C **83**, 025804 (2011).
[17] E. Massot, J. Margueron, and G. Chanfray, Europhys. Lett. **97**, 39002 (2012).
[18] P. Demorest, T. Pennucci, S. Ransom, M. Roberts, and J. Hessels, Nature (London) **467**, 1081 (2010).
[19] F. Hofmann, C. M. Keil, and H. Lenske, Phys. Rev. C **64**, 025804 (2001).
[20] L. Bonanno and A. Sedrakian, Astron. Astrophys. **539**, A16 (2012).
[21] S. Weissenborn, D. Chatterjee, and J. Schaffner-Bielich, Nucl. Phys. A **881**, 62 (2012).
[22] S. Weissenborn, D. Chatterjee, and J. Schaffner-Bielich, Phys. Rev. C **85**, 065802 (2012).
[23] I. Bednarek, P. Haensel, J. L. Zdunik, M. Bejger, and R. Manka, arXiv:1111.6942.
[24] R. Lastowiecki, D. Blaschke, H. Grigorian, and S. Typel, Acta Phys. Pol. B, Proc. Suppl. **5**, 535 (2012).
[25] M. Oertel, A. Fantina, and J. Novak, Phys. Rev. C **85**, 055806 (2012).
[26] R. Chrien and C. Dover, Annu. Rev. Nucl. Part. Sci. **39**, 113 (1989).
[27] J. Schaffner, C. B. Dover, A. Gal, C. Greiner, D. J. Millener, and H. Stocker, Ann. Phys. (NY) **235**, 35 (1994).
[28] A. Gal, Prog. Theor. Phys. Suppl. **186**, 270 (2010).
[29] P. K. Saha *et al*., Phys. Rev. C **70**, 044613 (2004).
[30] I. Sagert, M. Wietoska, J. Schaffner-Bielich, and C. T. Sturm, J. Phys. G **35**, 014053 (2008).
[31] I. Sagert, L. Tolos, D. Chatterjee, J. Schaffner-Bielich, and C. Sturm, arXiv:1111.6058.
[32] I. Vidana, D. Logoteta, C. Providencia, A. Polls, and I. Bombaci, Europhys. Lett. **94**, 11002 (2011).
[33] N. Glendenning, Phys. Rep. **342**, 393 (2001).
[34] A. Lavagno, Phys. Rev. C **81**, 044909 (2010).
[35] L. Yang, W. L. Qian, R.-K. Su, and H. Q. Song, Phys. Rev. C **70**, 045207 (2004).
[36] L. Yang, S. Y. Yin, W. L. Qian, and R.-K. Su, Phys. Rev. C **73**, 025203 (2006).
[37] K. Nakazato, S. Furusawa, K. Sumiyoshi, A. Ohnishi, S. Yamada, and H. Suzuki, Astrophys. J. **745**, 197 (2012).
[38] E. O'Connor and C. D. Ott, Astrophys. J. **730**, 70 (2011).
[39] S. Balberg and A. Gal, Nucl. Phys. A **625**, 435 (1997).
[40] K. Nakazawa (KEK-E176 and J-PARC-E07), Nucl. Phys. A **835**, 207 (2010).
[41] I. Vidana, D. Logoteta, C. Providencia, A. Polls, and I. Bombaci, arXiv:1004.3958.
[42] C. Ducoin, P. Chomaz, and F. Gulminelli, Nucl. Phys. A **789**, 403 (2007).
[43] C. Ducoin, C. Providencia, A. M. Santos, L. Brito, and P. Chomaz, Phys. Rev. C **78**, 055801 (2008).
[44] I. Vidana, A. Polls, A. Ramos, and M. Hjorth-Jensen, Nucl. Phys. A **644**, 201 (1998).
[45] C. Ducoin, P. Chomaz, and F. Gulminelli, Nucl. Phys. A **771**, 68 (2006).
[46] H. M. Antia, Astroph. J. Suppl. **84**, 101 (1993).
[47] J. Margueron, J. Navarro, and P. Blottiau, Phys. Rev. C **70**, 028801 (2004).